Continuous Mesoporous Pd Films by Electrochemical Deposition in Nonionic Micellar Solution

*Muhammad Iqbal[1,2], Cuiling Li[1], Kathleen Wood[3], Bo Jiang[1], Toshiaki Takei[1], Ömer Dag[4,5], Daisuke Baba[1,2], Asep Sugih Nugraha[1,2], Toru Asahi[2], Andrew E. Whitten[3], Md. Shahriar A. Hossain[6], Victor Malgras[1], and Yusuke Yamauchi[*1,2,6]*

1 International Center for Materials Nanoarchitectonics (MANA), National Institute for Materials Science (NIMS), 1-1 Namiki, Tsukuba, Ibaraki 305-0044, Japan.

2 Faculty of Science and Engineering, Waseda University, 3-4-1 Okubo, Shinjuku, Tokyo 169-8555, Japan.

3 Australian Centre for Neutron Scattering, Australian Nuclear Science and Technology Organisation (ANSTO), Lucas Heights, NSW 2234, Australia.

4 Department of Chemistry, Bilkent University, Ankara 06800, Turkey.

5 UNAM-National Nanotechnology Research Center and Institute of Materials Science and Nanotechnology, Bilkent University, Ankara 06800, Turkey.

6 Australian Institute for Innovative Materials (AIIM), University of Wollongong, Squires Way, North Wollongong, NSW 2500, Australia.

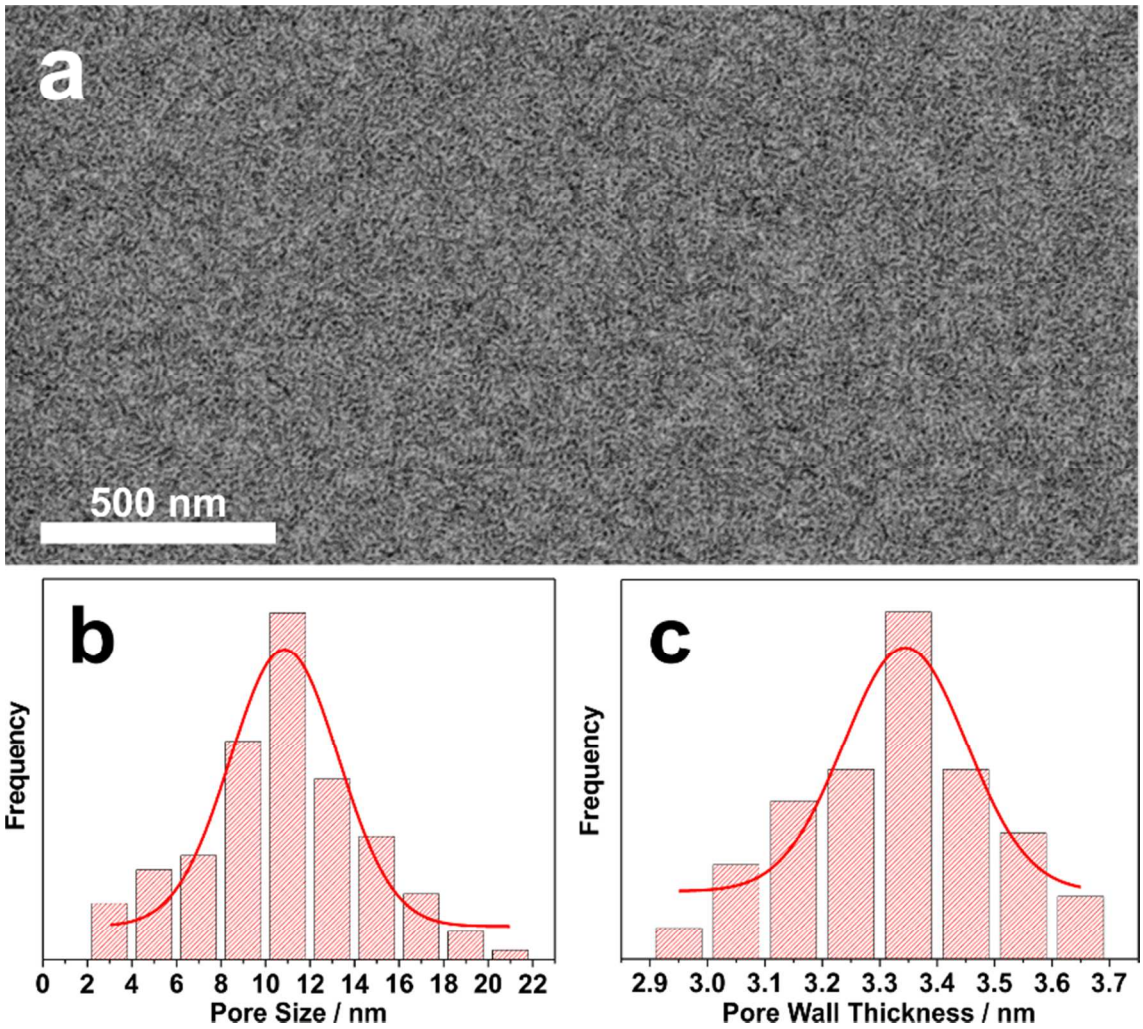

Figure S1. (a) Low-magnification SEM image of the film surface. Distribution histograms of (b) pore size and (c) pore wall thickness of a mesoporous Pd film prepared under typical conditions.

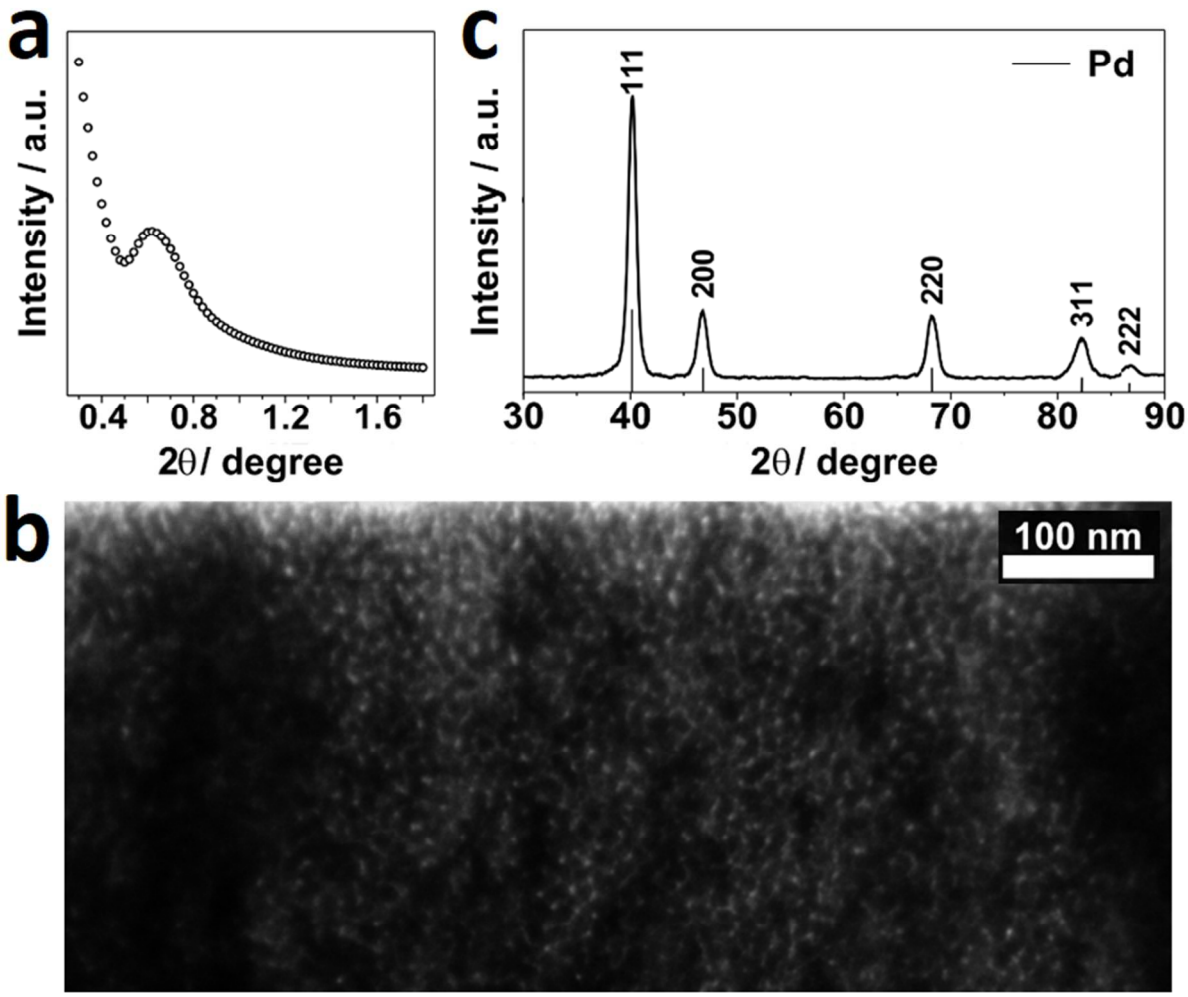

Figure S2. (a) Low-angle X-ray diffraction pattern, (b) bright-field cross-sectional TEM image, and (c) wide-angle X-ray diffraction pattern of a mesoporous Pd film prepared under the typical condition.

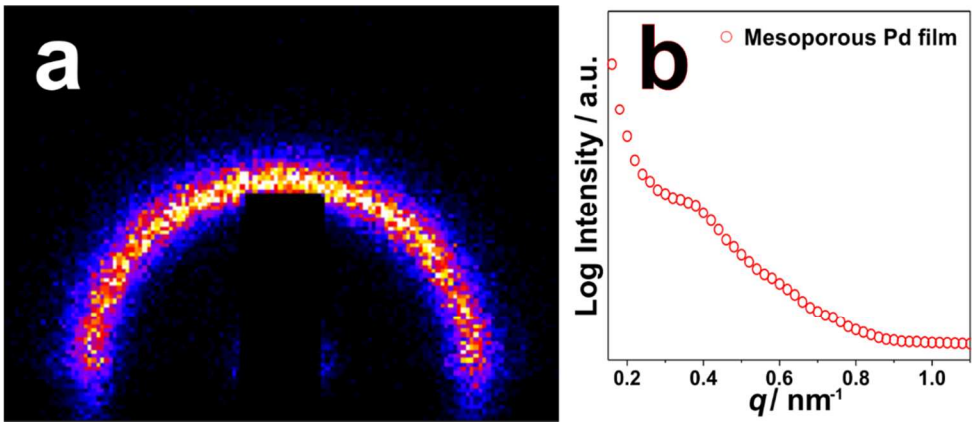

'S3'

Figure S1. (a) GI-SAXS pattern and (b) in-plane profile of a mesoporous Pd film prepared under the typical condition.

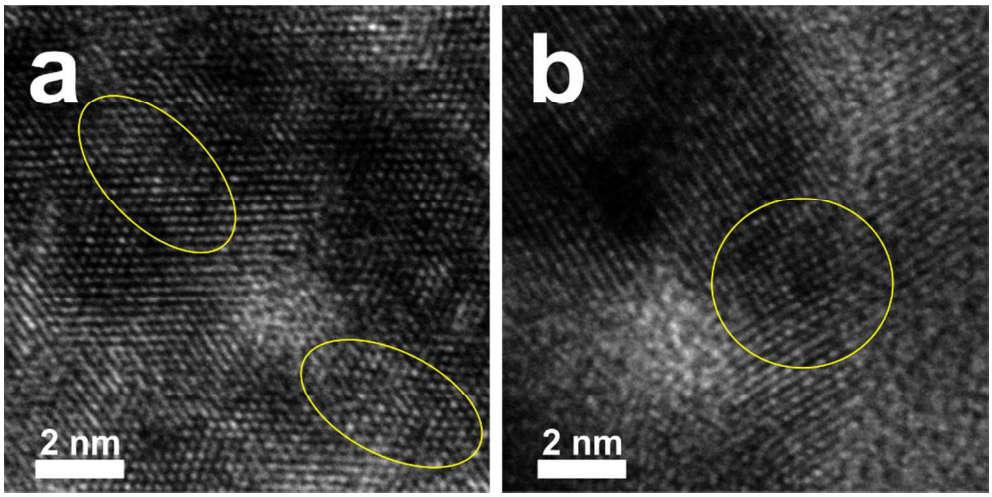

Figure S4. High-resolution TEM (HRTEM) images within the mesoporous Pd film. The yellow circle/ellipses showing the lattice fringes continuously spanning throughout several particles.

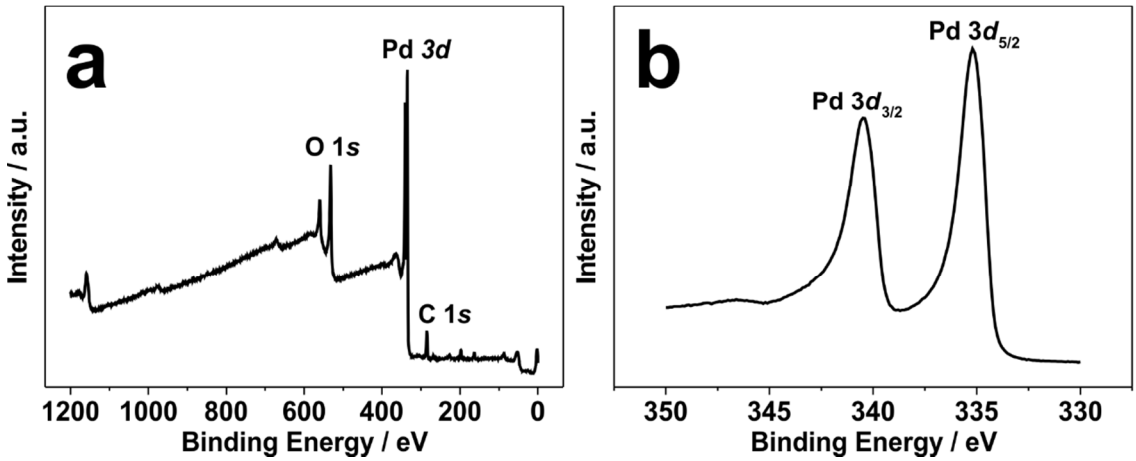

Figure S5. XPS spectra for mesoporous Pd film prepared under the typical condition. [(a) Full spectrum and (b) Pd3*d* spectrum]

Small angle neutron scattering on micellar solutions (Figure S6-S8)

P123 solutions with and without $PdCl_2$ metal precursor were first prepared in deuterated solvents and diluted until small angle neutron scattering data showed no micellar interactions. Deuterated solvents were used to enhance contrast and reduce background. The required final concentrations were found to be 0.5 wt%. Although the critical micelle temperature (CMT) varies with the concentration, the micellar structure is expected to be the same at the same temperature difference from the CMT at different concentrations[R1], *i.e.*, P123 micelles in a 0.5 wt% solution at 25°C are expected to be the same as those in a 2.5 wt% solution at 20°C.[R2]

The forward scattered intensity (*I(0)*) measured by SANS is related to the aggregation number (N_{agg}) via the relationship:

$$\left(\frac{I(0)}{(C-CMC)}\right)^{0.5} = {N_{agg}}^{0.5}(b_m - V_m\rho_s) \quad (1)$$

Where C is the concentration, b_m the unimer scattering length, V_m the unimer volume and ρ_s the solvent scattering length density.[R1, R3] Varying the solvent scattering length density by changing the D_2O/H_2O ratio in the solvent therefore allows the calculation of the unimer volume and micelle aggregation number. Both samples (with and without $PdCl_2$) were therefore measured at 40, 60, 80, 100 % D_2O.

All samples were placed in a temperature controlled sample block and recorded at three temperatures above the CMT. The final temperature in the sample block was recorded.

To establish the quality of the data collected, the radii of gyration (*Rg*) and the forward scattering intensity (*I(0)*) were calculated from both the Guinier analysis and the radial probability distribution function using Primus[R4]. For all samples measured, the extracted values agree within error. Probability distribution functions for all samples were calculated using Primus[R4] and were found to be consistent with a spherical shape. Those without metal precursor are shown as an example in **Figure S6**.

The radius of gyration is a model independent parameter extracted from SANS data, and assuming a spherical particle, is related to the diameter of the particle (D) through the relation:

$$D = 2\sqrt{\frac{5}{3}}R_g \quad (2)$$

Diameters of P123 micelles calculated from the radius of gyration using (1) are plotted in **Figure S7**. The values are slightly larger than those calculated from fitting the full scattering curve, probably due to the distribution of sizes in solution and the larger particles having a larger contribution to the calculated radius of gyration. A very small decrease in the size of the P123 micelles (~0.1 nm) is observed at all temperatures upon addition of the $PdCl_2$, as can be seen in **Figure S7**. Upon increasing temperature, the overall size of the micelles increases by less than 1 nm, as can be seen in extracted particle diameters in **Figure S7**. Scattering curves and extracted probability distribution functions are consistent with an unchanged spherical shape. The linear fit presented in **Figure S8** allows the determination of a P123 unimer volume and the aggregation number of the micelles in solution. At 25°C the volume of the unimer was calculated to be 5,520 $Å^3$ and an aggregation number of 309 was determined.

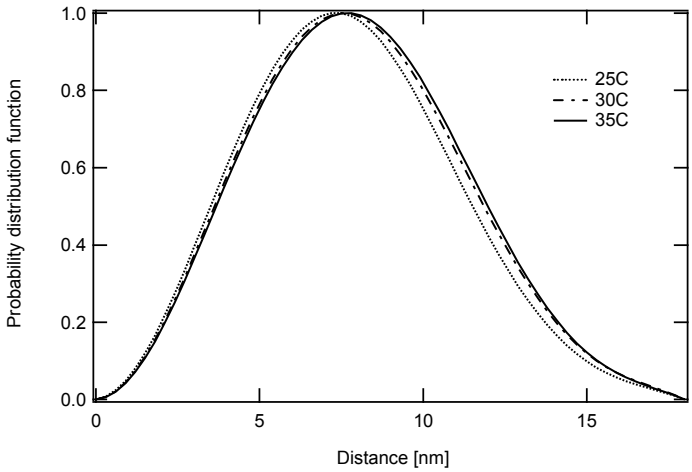

Figure S6. Probability distribution functions as a function of temperature for P123 samples at 0.5 wt% in 100 % D_2O.

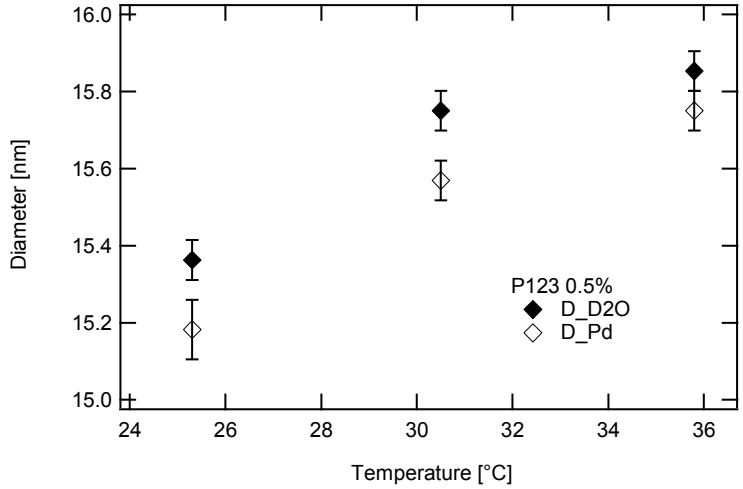

Figure S7. Temperature dependence of the diameter of P123 micelles in solution, extracted from the *P(r)* analysis, assuming a spherical particle, with and without metal precursor.

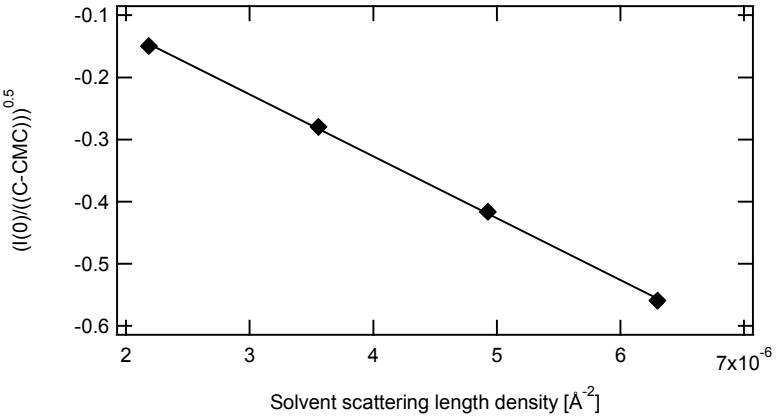

Figure S8. Linear fit of $\left(\frac{I(0)}{(C-CMC)}\right)^{0.5}$ versus solvent scattering length density at 25°C.

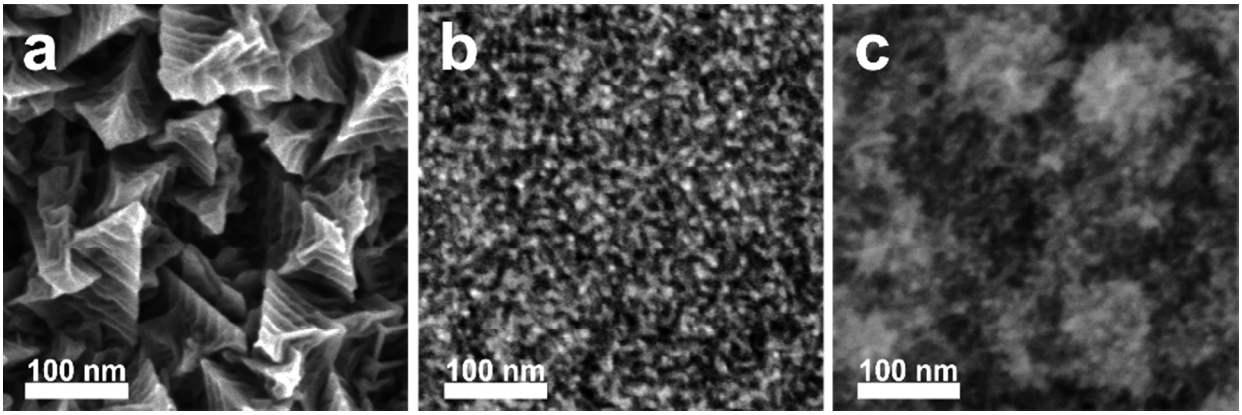

Figure S9. Top-view SEM images of Pd films prepared (a) without surfactant, (b) with 2.5 wt% F127, and (c) with 2.5 wt% Brij 58.

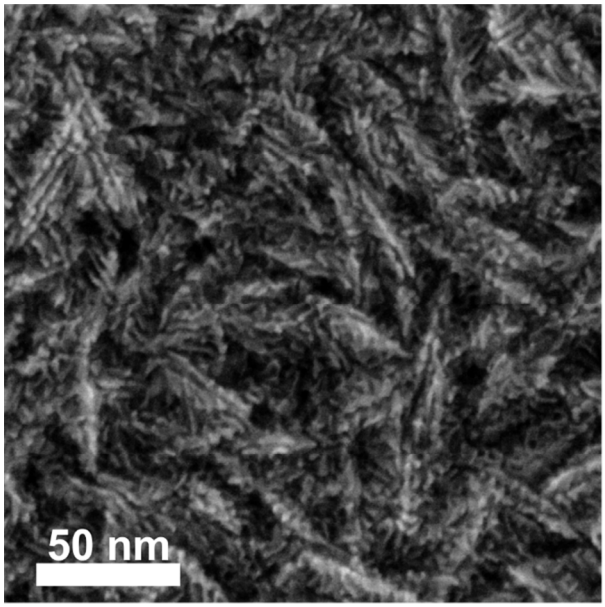

Figure S10. SEM images of the Pd film prepared with an applied potential of 0.1 V (*vs.* Ag/AgCl).

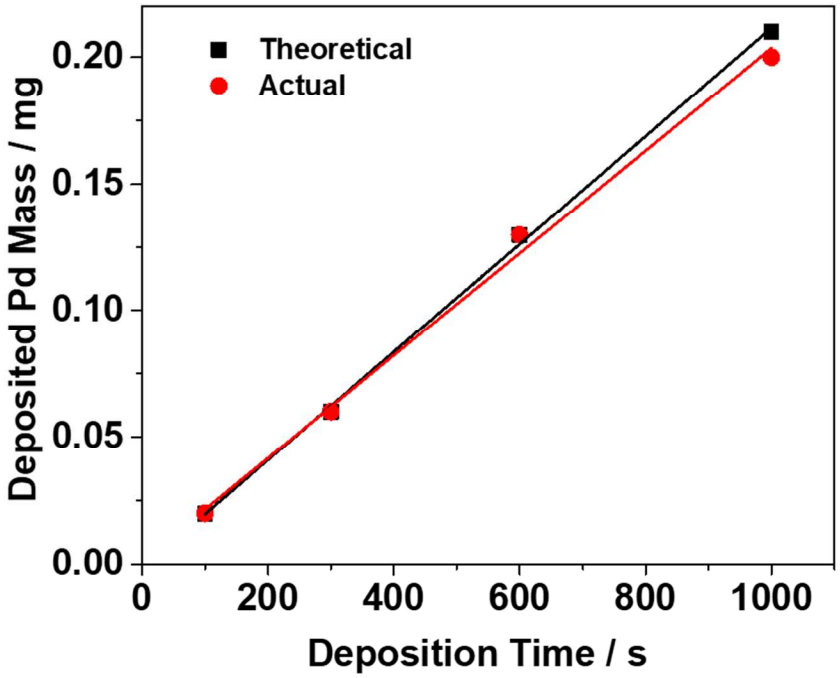

Figure S11. Relationship between Pd mass deposited on the working electrode and the deposition time calculated by theoretical approach and measured with a precision balance.

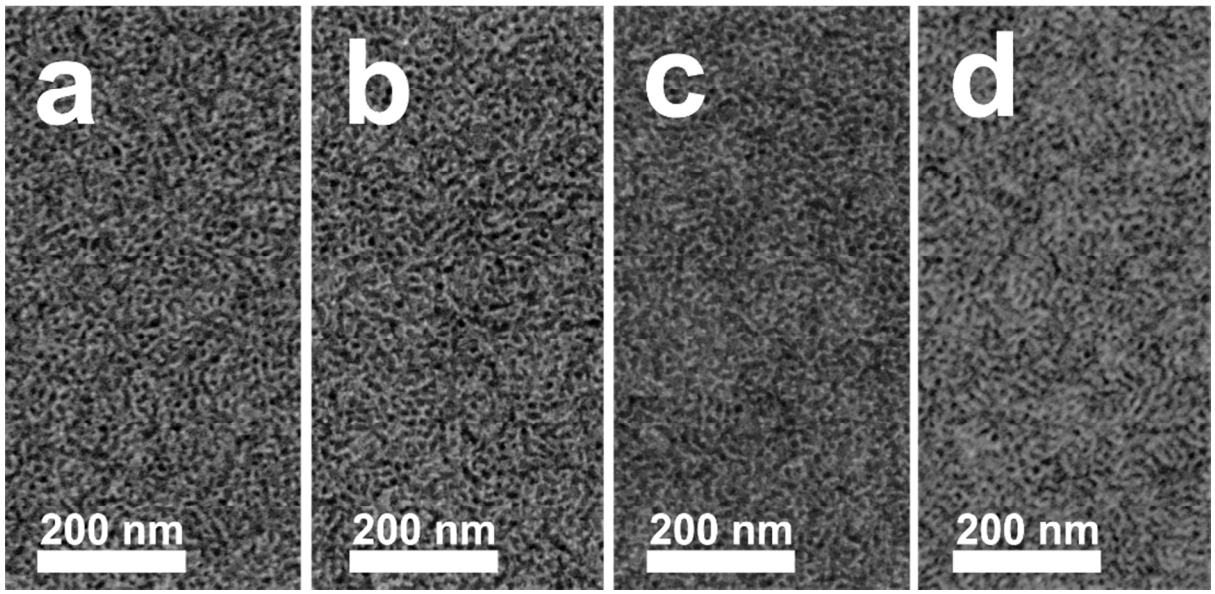

Figure S12. Time-evolution of mesoporous Pd films morphology prepared at various applied deposition time: (a) 6 s, (b) 16 s, (c) 100 s and (d) 600 s.

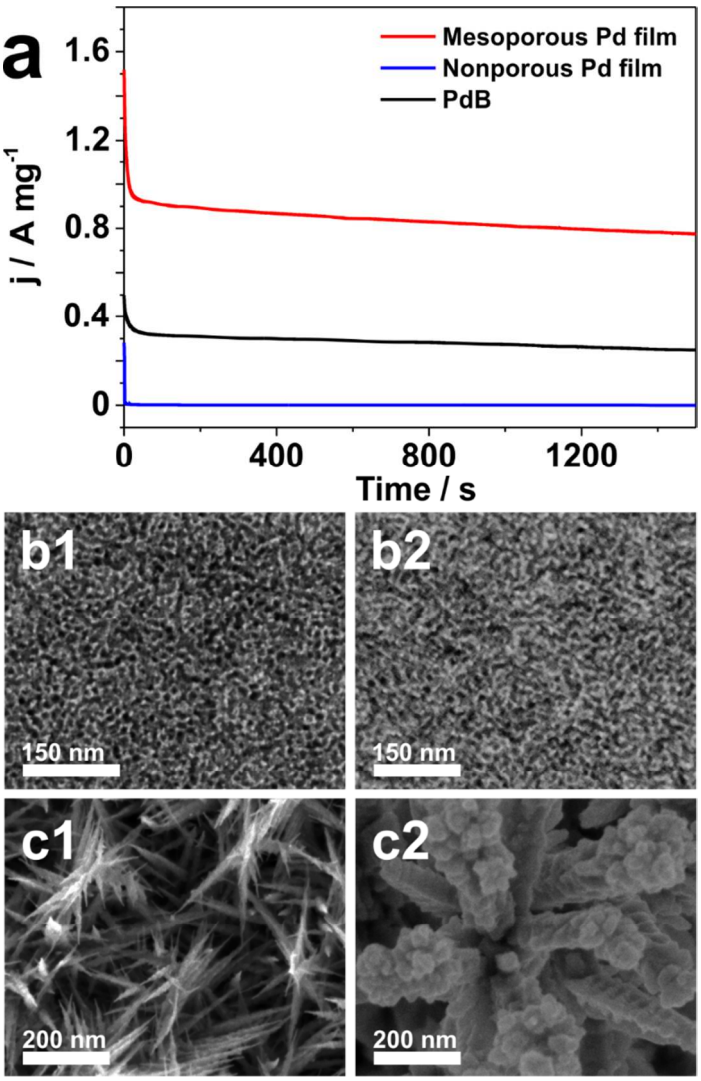

Figure S13. (a) Amperometric *i-t* curve of mesoporous Pd film, nonporous Pd film and PdB for the catalytic stability test at potential of -0.3 V for 1500 s. SEM images of (b) mesoporous Pd film and (c) nonporous Pd films before and after the stability test.

Table S1. Mesoporous materials prepared by the assistance of Pluronic P123 as a template.

No.	Sample Name	Surfactant	Pore Size (nm)	Ref.
1	Mesoporous silica	P123	10.2	R5
2	Porous titania thin film	P123	9-12	R6
3	Pore-expanded mesoporous silica (S-H1)	P123	11.3	R7
4	Mesoporous silica rod	P123	11.2	R8
5	MSU-H silica	P123	7.6-11.9	R9

REFERENCE

[R1] Goldmints, I.; von Gottberg, F. K.; Smith, K. A.; Hatton, T. A. Small-Angle Neutron Scattering Study of PEO-PPO-PEO Micelle Structure in the Unimer-to-Micelle Transition Region. *Langmuir* **1997**, *13*, 3659-3664.

[R2] Alexandridis, P.; Holzwarth, J. F.; Hatton, T. A. A Correlation for the Estimation of Critical Micellization Concentrations and Temperaturse of Polyols in Aqueous Solutions. *J. Am. Oil Chem. Soc.* **1995**, *72*, 823-826.

[R3] Chen, S. H. Small Angle Neutron Scattering Studies of the Structure and Interaction in Micellar and Microemulsion Systems. *Annu. Rev. Phys. Chem.* **1986**, *37*, 351.

[R4] Konarev, P. V.; Volkov, V.V.; Sokolova, A.V.; Koch, M. H. J.; Svergun, D. I. PRIMUS - a Windows-PC based system for small-angle scattering data analysis. *J Appl Cryst.* **2003**, *36*, 1277-1282.

[R5] Feng, P.; Bu, X.; Pine, D. J. Control of Pore Sizes in Mesoporous Silica Templated by Liquid Crystals in Block Copolymer-Cosurfactant-Water Systems. *Langmuir* **2000**, *16*, 5304-5310.

[R6] Wu, Q. L.; Subramanian, N.; Rankin, S. E. Hierarchically Porous Titania Thin Film Prepared by Controlled Phase Separation and Surfactant Templating. *Langmuir* **2011**, *27*, 9557–9566.

[R7] Ma, J.; Liu, Q.; Chen, D.; Wen, S.; Wang, T. Synthesis and Characterisation of Pore-expanded Mesoporous Silica Materials. *Micro & Nano Letters* **2014**, *10*, 140-144.

[R8] Johansson, E. M.; Ballem, M. A.; Córdoba, J. M.; Odén, M. Rapid Synthesis of SBA-15 Rods with Variable Lengths, Widths, and Tunable Large Pores. *Langmuir* **2011**, *27*, 4994-4999.

[R9] Kim, S. S.; Karkamkar, A.; Pinnavaia, T. J. Synthesis and Characterization of Ordered, Very Large Pore MSU-H Silicas Assembled from Water-Soluble Silicates. *J. Phys. Chem. B* **2001**, *105*, 7663-7670.